# Mechanistic model for stresses in the oxide layer formed on zirconium alloys

I. Gupta, J. R. Barber, M. D. Thouless, W. Lu

*Department of Mechanical Engineering,*

*University of Michigan,*

*Ann Arbor, MI 48109*

**Abstract**

Zirconium alloys are widely used as the cladding material in pressurized-water-reactors. The oxide formed is subjected to compressive stresses which relax over time. This may affect the protectiveness of the oxide layer by allowing crack formation. We present a mechanistic model to predict these stresses as a function of temperature and oxidation kinetics. Material parameters for elastic deformation, creep, and thermal expansion are taken from appropriate experimental studies and the resulting predictions for the evolution of the stress distributions are compared with other experimental data. Dislocation glide in the oxide is found to be the dominant mechanism of stress relaxation for temperatures below 900 K.

# Introduction

Zirconium alloys are used as the cladding material for fuel rods in a Pressurized-Water Reactor (PWR) because of their low neutron-absorption capability and their resistance to high-temperature corrosion and radiation damage. The cladding undergoes oxidation while being exposed to the pressurized water used as a coolant in a PWR. Oxide films formed on zirconium alloys are subjected to in-plane compressive stresses associated with a Pilling-Bedworth ratio of 1.56 [1]. The compressive stress and the good adherence between the oxide and substrate make these films inherently protective in nature, because the compressive stress prevents the formation of cracks which could provide a low resistance path for diffusion of the oxidizing species. However, despite the compressive stress, transitions in the nature of the oxide and its kinetics have been observed [2]. The resultant accelerated oxidation rates lead to an increase in the amount of hydrogen entering the zircaloy, and embrittlement by the resultant formation of hydrides, which can place limits on the fuel burn-up in reactors.

The monoclinic phase of zirconia is thermodynamically stable below 1400 K, above which the tetragonal phase is stable up to 2600 K. However, phase-characterization studies [3, 4, 5, 6] show that there is a high density of the tetragonal phase in the oxide film, even at temperatures below 1000 K. It is recognized that the high compressive stresses within the oxide may be a contributing factor to this observation [7]. Experiments show that both the volume fraction of the tetragonal phase and the compressive stresses in the oxide decrease continuously with time, and this phase transformation has been postulated as a possible trigger for a transition in the oxidation kinetics of zirconium alloys [8].

Since the oxide stresses play an important role in these processes, we would like to be able to predict the evolution of the stress field under varying mechanical and thermal conditions. This is the objective of the present paper.

# Statement of the problem

We consider the problem illustrated in Fig. 1 in which a plane sheet is oxidized on both sides, since this geometry has been used in several experimental studies [3, 6, 9]. We shall argue later that the methods developed are easily applied to other geometries more representative of practical PWR systems. We

assume that the oxide film thickness $h_{\text{ox}}(t)$ and the [spatially uniform] temperature $T(t)$ are known functions of time $t$, and we wish to predict the evolution of the corresponding stress field. We assume that $h_{\text{ox}}(t)$ is independent of $x$, but experimental observations [10, 11] show significant irregularities in the oxide-metal interface. These can be expected to generate corresponding perturbations in the stress field local to the interface [12].
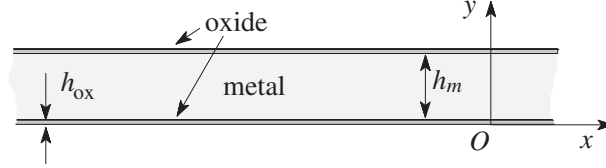


Figure 1: Two-sided oxidation of a thin sheet specimen

We define a coordinate system such that the $y$-axis is perpendicular to the plate surfaces and $x$ and $z$ are in-plane directions. The symmetric geometry implies that no bending occurs and hence the in-plane strains $\epsilon_{xx}(t), \epsilon_{zz}(t)$ are independent of $y$. The sheet is free to expand in both $x$ and $z$-directions, so these strain components must be equal and the corresponding stress state is also biaxial — i.e.

$$\epsilon_{xx} = \epsilon_{zz} \equiv \varepsilon(t) \quad \text{and} \quad \sigma_{xx} = \sigma_{zz} \equiv s(y,t) \; ; \quad \sigma_{yy} = 0 \tag{1}$$

which serves to define the in-plane biaxial stress $s(y,t)$ and strain $\varepsilon(t)$. Notice that in the oxide, $s(y,t)$ is a function of both $y$ and $t$, since different regions of the oxide are generated at different times, whereas in the metal, $s(t)$ is a function of $t$ only.

Since no forces are applied to the sheet, the mean value of $s(y,t)$ across the thickness must be zero for all $t$ — i.e.

$$\int_0^h s(y,t)dy = 0 , \quad \text{where} \quad h = h_{\text{m}} + 2h_{\text{ox}} \tag{2}$$

This equilibrium condition and the constitutive laws for the materials [i.e. the relations between stress, strain and temperature] are sufficient to determine $s(y,t)$ for given $h_{\text{ox}}(t), T(t)$.

3

# Material behaviour

Strain components in both metal and oxide can be anticipated due to (1) elastic deformation, (2) thermal strain, and (3) inelastic deformation, notably creep. We shall consider each of these contributions separately and draw on published experimental data to decide on appropriate functional forms and material properties. The properties of the metal substrate are generally well-documented, though creep mechanisms can be quite complex [13]. By contrast, oxide properties are complicated by the fact that the oxide involves a mixture of two phases, both of which are anisotropic.

## Elastic deformation

For Zircaloy-4, Polatidis *et al.* [3] quote the values $E_m = 96$ GPa, $\nu_m = 0.34$, where $E$ and $\nu$ are Young's modulus and Poisson's ratio, respectively. Since elastic properties for alloys are relatively insensitive to small changes in composition, we shall also use these values for ZIRLO. For the oxide, the same authors give the values $E_{ox} = 253$ GPa, $\nu_{ox} = 0.282$.

## Thermal strain

Guerain *et al.* [14] give a value of $\alpha_m = 5.8 \times 10^{-6}$ K$^{-1}$ for the thermal-expansion coefficient of the substrate. For monoclinic zirconia, the thermal-expansion coefficient varies between $1.2 \times 10^{-6}$ K$^{-1}$ and $12.6 \times 10^{-6}$ K$^{-1}$, depending on the crystal orientation [4], so the degree of uncertainty introduced by these factors is quite large. However, these authors report XRD studies for a sheet specimen oxidized as in Fig. 1, after which the temperature was cycled between $T = 743$ K and $T = 293$ K. Under these conditions, the equilibrium condition (2) and strain compatibility imply that the in-plane stress in the oxide should change by

$$\Delta s_{ox} = (\alpha_m - \alpha_{ox}) \Delta T \left/ \left[ \frac{(1 - \nu_{ox})}{E_{ox}} + \frac{2h_{ox}}{h_m} \frac{(1 - \nu_m)}{E_m} \right] \right. \tag{3}$$

where $\Delta T$ is the change in temperature. Using this result and elastic properties from "Elastic deformation" Section, the XRD data from [4] imply a thermal expansion coefficient $\alpha_{ox} = 5 \times 10^{-6}$ K$^{-1}$. However, in view of the uncertainty of oxide composition and orientation, we here use values in the range $\alpha_{ox} = 5 \pm 2 \times 10^{-6}$ K$^{-1}$.

4

## Substrate creep

Wang *et al.* [13] developed a deformation-mechanism map for creep of Zircaloy-4, based on a comprehensive survey of published experimental data. For temperatures and stress levels in typical PWR applications, the dominant mechanisms are diffusional creep and power-law creep. The power-law creep mechanism exhibits a relationship between the von Mises effective normal stress, $\sigma_{\mathrm{eq}}$, and the effective normal strain rate $\dot{\epsilon}_{\mathrm{eq}}$ of the form [13]

$$\dot{\epsilon}_{\mathrm{eq}} = \frac{AG}{T} \exp\left(-\frac{Q_p}{RT}\right) \left(\frac{\sigma_{\mathrm{eq}}}{G}\right)^{5.1} \tag{4}$$

where $Q_p = 285 \pm 20$ kJ/mol is the activation energy, $T$ is the absolute temperature, $R$ is the molar gas constant, and the shear modulus $G = (39400 - 13.4T)$ MPa. Wang *et al.* [13] estimate the constant $A$ as $2.1 \times 10^{24}$ K MPa$^{-1}$ s$^{-1}$, based on a wide range of experimental studies, though outliers in this data correspond to values with upper and lower bounds $5.2 \times 10^{24}$ K MPa$^{-1}$ s$^{-1}$ and $7 \times 10^{23}$ K MPa$^{-1}$ s$^{-1}$ respectively. Because of the 5.1 power, the predicted stresses are rather weak functions of $A$, so variation within this range has comparatively little effect on the results.

Diffusional creep is generally assumed to follow a linear relation [15]

$$\dot{\epsilon}_{\mathrm{eq}} = \frac{B\sigma_{\mathrm{eq}}}{T} \exp\left(-\frac{Q_d}{RT}\right) \tag{5}$$

Data for diffusional creep parameters for Zr-4 is sparse, but using experimental data from Kaddour *et al.* [16] [based on specimens with an average grain dimension of 8 $\mu$m] and $Q_d = 190$ kJ/mol [16], the constant $B$ can be estimated as $B = 1.76 \times 10^6$ K MPa$^{-1}$ s$^{-1}$.

The strain-rate tensor is related to $\dot{\epsilon}_{\mathrm{eq}}$ by

$$\dot{\epsilon}_{ij} = \frac{3\sigma'_{ij}}{2\sigma_{\mathrm{eq}}} \dot{\epsilon}_{\mathrm{eq}} \tag{6}$$

where $\sigma'_{ij} = \sigma_{ij} - \sigma_{kk}/3$ is the deviatoric component of the stress tensor. For the particular case of

in-plane biaxial stress $\sigma_{xx} = \sigma_{zz} = s$, $\sigma_{\mathrm{eq}} = |s|$ and the in-plane creep strain rate is

$$\dot{\varepsilon} = \frac{3}{2|s|}\left(s - \frac{2s}{3}\right)\dot{\epsilon}_{\mathrm{eq}} = \mathrm{sgn}(s)\frac{\dot{\epsilon}_{\mathrm{eq}}}{2} \tag{7}$$

where $\mathrm{sgn}(s) = s/|s|$ is the signum function, equal to $+1$ if $s > 0$ and $-1$ if $s < 0$.

## Oxide creep

We are not aware of published creep data for the oxide formed on zircaloy, so we here assume that this can reasonably be approximated by data for other forms of zirconia [15]. In particular, we note that diffusional creep will be of negligible significance compared with other creep mechanisms at the compressive stresses typically exhibited in the oxide layer [17].

Platt *et al.* [6] assumed the Coble-creep law proposed by Choksi *et al.* [17] for stabilized-tetragonal zirconia, and showed that this mechanism had negligible impact on the oxide stresses. However, the possibility of other creep mechanisms was not considered. In particular, it should be noted that the high compressive stresses that occur in an oxide film suppress brittle fracture. This permits deformation mechanisms associated with dislocation motion to occur, such as dislocation glide and power-law creep. Indeed, experimental studies [18] have indicated that such plastic deformation occurs both in the oxide films formed on zirconium alloys and in pure monoclinic zirconia.

Based on these arguments, we assume that deformation occurs by dislocation glide, for which we use the generic model

$$\dot{\epsilon}_{\mathrm{eq}} = \dot{\epsilon}_0 \exp\left[-\frac{Q_g}{RT}\left(1 - \frac{\sigma_{\mathrm{eq}}}{\sigma_g}\right)\right] \tag{8}$$

[15]. In this equation, the yield strength at 0 K is taken to be $\sigma_g = 7800$ MPa, and the activation energy is $Q_g = 173.5$ kJ/mol, as reported for lattice-resistance-controlled dislocation-glide in yttria-stabilized cubic zirconia by Baufeld *et al.* [19]. We shall estimate the pre-exponential coefficient $\dot{\epsilon}_0$ in Section "Estimation of $\dot{\epsilon}_0$" below, using oxide strain measurements at 633 K from Polatidis *et al.* [3], but first we need to discuss the stress state under which the oxide is formed.

## Oxide growth strains

Zirconium oxide has a higher molar volume than zirconium, so a biaxial compressive stress is developed in the oxide film owing to the constraint exerted by the substrate while the oxide forms. The Pilling-Bedworth ratio, $V_{PB}$, defined as the ratio of the molar volume of the oxide to the molar volume of the metal, is equal to 1.56 for zirconium oxide [1]. If the volumetric expansion during unrestrained growth is assumed to be isotropic, the resulting compressive strain within the oxide would be given by $((V_{PB})^{1/3} - 1) = 0.16$, implying in-plane compressive stresses within the oxide of around 57 GPa. It can be seen that substitution of such stress levels into Eqn. 8 results in huge plastic strain rates, implying a very rapid relaxation of stresses to more reasonable levels. Previous studies [6, 20] have assumed that the oxide forms at an in-plane compressive stress of about 2 GPa, but stresses as high as 4 GPa have been measured experimentally [21, 22], suggesting that the value 2 GPa is merely an arbitrary temporal point for a rapidly relaxing compressive stress. However, the precise details of how the stresses relax from the theoretical initial value is beyond the scope of this work.

# Calculation of stresses

Superposing strains from the various mechanisms discussed in Section "Material behaviour", we obtain the in-plane strain rates

$$\dot{\varepsilon}_{\mathrm{m}}(t) = \frac{\mathrm{sgn}(s_{\mathrm{m}}(t))}{2T}\left[AG\exp\left(-\frac{Q_p}{RT}\right)\left(\frac{|s_{\mathrm{m}}(t)|}{G}\right)^{5.1} + B\exp\left(-\frac{Q_d}{RT}\right)|s_{\mathrm{m}}(t)|\right]$$
$$+\frac{\dot{s}_{\mathrm{m}}(t)(1-\nu_{\mathrm{m}})}{E_{\mathrm{m}}} + \alpha_{\mathrm{m}}\dot{T} \tag{9}$$

$$\dot{\varepsilon}_{\mathrm{ox}}(t) = \frac{\mathrm{sgn}(s_{\mathrm{ox}}(y,t))\dot{\epsilon}_0}{2}\exp\left[-\frac{Q_g}{RT}\left(1-\frac{|s_{\mathrm{ox}}(y,t)|}{\sigma_g}\right)\right]$$
$$+\frac{\dot{s}_{\mathrm{ox}}(y,t)(1-\nu_{\mathrm{ox}})}{E_{\mathrm{ox}}} + \alpha_{\mathrm{ox}}\dot{T} \tag{10}$$

Notice that the in-plane strains and the stress in the metal substrate are functions of time only, but the stress in the oxide is a function of both the distance, $y$ from the oxide-air/water interface, and time $t$, since oxidation at different spatial points starts at different times. The initial condition for newly formed oxide was taken to be a compressive stress of 57 GPa, but because initial creep is very rapid, the results are not sensitive to the precise value chosen.

To complete the problem statement, we use the compatibility condition that the lateral strain rates in the oxide and substrate be equal for all times $t$ [i.e. $\dot{\varepsilon}_{\mathrm{ox}}(t) = \dot{\varepsilon}_{\mathrm{m}}(t) \equiv \dot{\varepsilon}(t)$], and the equilibrium condition (2).

## Estimation of $\dot{\epsilon}_0$

The values for the parameters required in this study were all taken directly from the experimental literature, as described in Section "Material behaviour", except for the pre-exponential coefficient $\dot{\epsilon}_0$ in Eqn. (8). To estimate this parameter, we performed a curve fit of the average stress in the oxide layer predicted by the model to *ex situ* measurements of residual stress reported by Polatidis *et al.* [3] for oxidation at a temperature of $T = 633$ K. The oxide growth law $h_{\mathrm{ox}}(t)$ for this case was obtained by fitting a smooth curve to the experimental data reported in [3].

The results are shown in Fig. 2. The points show the experimental results from [3] and the shaded region defines the bounds of the predictions based on Eqns. (9, 10), with $\dot{\epsilon}_0 = 300$ s$^{-1}$ and a thermal expansion coefficient of the oxide ($\alpha_{\mathrm{ox}}$) in the range $5 \pm 2 \times 10^{-6}$ K$^{-1}$.
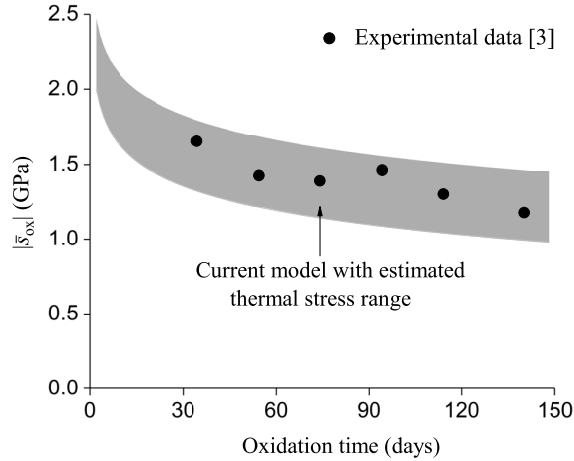


Figure 2: Estimation of the pre-exponential coefficient $\dot{\epsilon}_0$ in Eqn. (8), based on experimental data for the *ex situ* average in-plane compressive stress $|\bar{s}_{\mathrm{ox}}|$ in the oxide [3] at $T = 633$ K. The shaded region represents predicted results for chosen range of oxide's thermal expansion coefficient, $\alpha_{\mathrm{ox}} = 5 \pm 2 \times 10^{-6}$ K$^{-1}$.

The value of $\dot{\epsilon}_0 = 300$ s$^{-1}$ is much lower than that generally quoted in the literature ($\dot{\epsilon}_0 = 10^6$ s$^{-1}$) for a large set of materials [15]. Such values of $\dot{\epsilon}_0$ could have been achieved if we had chosen a

higher value of activation energy ($Q_g \sim 230$ kJ/mol instead of $Q_g = 173.5$ kJ/mol) while fitting our model to the experimental data of oxide stress in Fig 2. It is worth noting that Douglass [18] describes experiments showing that the hardness of cubic zirconia is significantly more temperature sensitive than is the monoclinic phase. This suggests that the activation energy for the oxide layer may be higher than that of cubic zirconia, used in this study. It is clear that further progress in understanding oxide stress relaxation at elevated temperatures is contingent on more direct experimental investigations of the creep behaviour of the oxide.

**An approximate solution**

In many applications, the oxide layer is much thinner than the metal $[h_{\text{ox}} \ll h_{\text{m}}]$, in which case the equilibrium condition (2) implies that the in-plane stresses in the metal are low, even when those in the oxide are high. If the corresponding contributions to the in-plane strain rate $\dot{\varepsilon}_{\text{m}}(t)$ are sufficiently small to be approximated as zero, equations (9, 10) and the compatibility condition then reduce to

$$
\frac{\text{sgn}(s_{\text{ox}}(y,t))\dot{\epsilon}_0}{2} \exp\left[-\frac{Q_g}{RT}\left(1 - \frac{|s_{\text{ox}}(y,t)|}{\sigma_g}\right)\right]
$$
$$
+ \frac{\dot{s}_{\text{ox}}(y,t)(1-\nu_{\text{ox}})}{E_{\text{ox}}} + (\alpha_{\text{ox}} - \alpha_{\text{m}})\dot{T} = 0 \tag{11}
$$

If the temperature $T$ is constant and $s_{\text{ox}}$ is always compressive, this equation can be solved in closed form giving

$$
\exp\left(\frac{Q_g s_{\text{ox}}}{RT\sigma_g}\right) = \exp\left(\frac{Q_g s_0}{RT\sigma_g}\right) + \frac{Q_g E_{\text{ox}}\dot{\epsilon}_0\, t}{2RT\sigma_g(1-\nu_{\text{ox}})}\exp\left(-\frac{Q_g}{RT}\right) \tag{12}
$$

where $s_0 = -57$ GPa is the in-plane stress at the instant at which a given layer of oxide was formed, and time $t$ is measured from that instant. Notice that because of the extremely rapid creep at small values of $t$, the predictions at practical time scales are quite insensitive to the value of $s_0$.
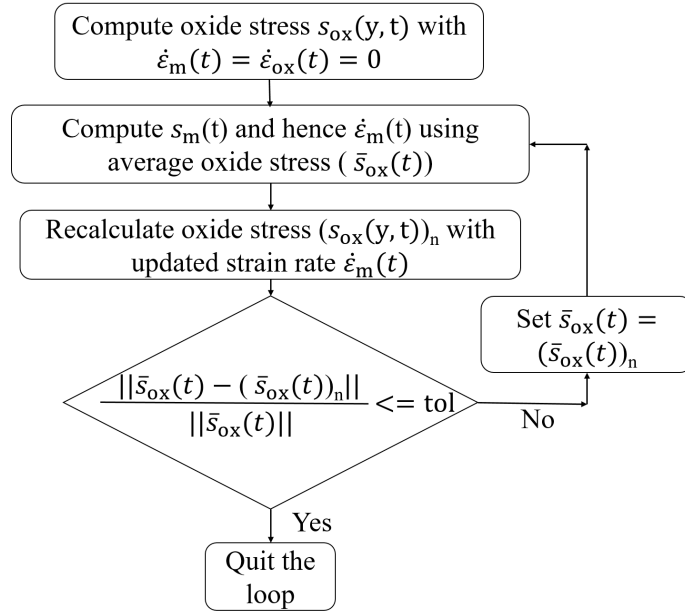
Figure 3: An iterative procedure for the simultaneous solution of Eqns. (9, 10).

If the strains in the substrate are small but not negligible, the solution of Eqn. 11 can be used as the first step of an iterative procedure. Using the approximation for $s_{\mathrm{ox}}(y,t)$ from that equation, we estimate $s_m(t)$ from Eqn. (2) and substitute this value into Eqn. 9 to obtain an improved estimate for the strain rate of the substrate, $\dot{\varepsilon}_{\mathrm{m}}(t)$. Repetition of this procedure, as shown in the flowchart of Fig. 3, allows results to be obtained to any desired degree of accuracy.

# Results

In this section, we shall compare the predictions of the model with experimental results for oxide stresses from two previous studies.

Platt *et al.* [6] used synchrotron X-ray diffraction [S-XRD] to obtain the in-plane stress, $s$, *in situ* while samples were being oxidized at two different temperatures of 923 K and 983 K. The volume fractions, $f_T$ and $f_M$, of the tetragonal and monoclinic phases, respectively, and the corresponding stresses, $s_T$ and $s_M$, were measured using S-XRD and these values were then used to determine the average oxide stress, defined as

$$s_{\mathrm{ox}} = f_T s_T + f_M s_M \tag{13}$$

In these experiments, temperatures were reported to increase from an initial value of 563 K at a rate of $\sim$ 11.2 K/min, until the required temperature was achieved. Thus, conditions for both experiments were nominally identical until t = 32 min, after which the temperature continued to rise in the 983 K case only. The oxide growth law $h_{ox}(t)$ for each case was determined by interpolating smooth curves through the experimental values from [6], including an initial transient for the initial heating phase, for which no experimental values were reported.
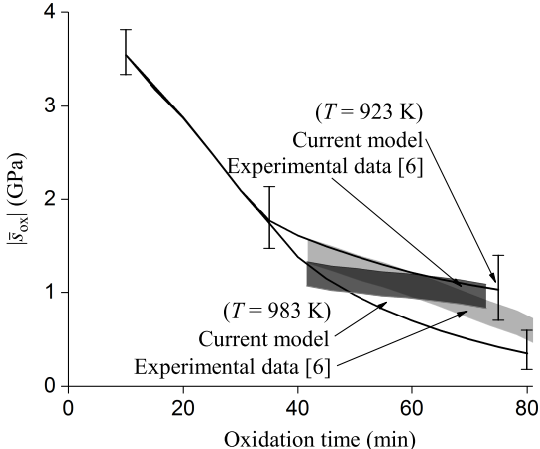


Figure 4: Comparison of predictions of average in-plane oxide compressive stress ($|\bar{s}_{ox}|$) at $T = 923$ K and $T = 983$ K with *in-situ* experimental data from [6]. Error bars show the effect of uncertainty in the model parameters.

Experimental oxide stress values are compared with predictions from the current model in Fig. 4. Uncertainty in the power-law creep parameters of zircaloy-4 and glide parameters for the oxide, quantified in previous sections, is represented by error bars in this figure.

Figure 4 shows that the model predictions agree well with the experimental data, in view of the range of uncertainty of the model parameters. In particular, the trend [slope] of the predictions is very close to the experimental data, indicating that the assumed creep laws and parameters describe the evolution of the system correctly.

The most significant discrepancy is the overprediction of the 'starting' value of stress at $t = 41$ min for $T = 923$ K. We recall that conditions for both experiments were nominally identical until $t = 32$

11

min, after which the temperature continued to rise in the 983 K case only. Since creep rate is a strong function of temperature, this suggests that the stresses at 983 K should if anything be lower than those at 923 K, but the opposite was reported in the earlier stages of measurement. We note however that similar experiments in the same study using ZIRLO specimens [6] did not replicate this behaviour. The low intensity of the diffracted X-ray beam from relatively thin oxide layers poses a significant constraint on the accurate measurement of the lattice strains during the early stages of oxidation, so this discrepancy should perhaps not be given undue weight.

## Effect of substrate strain

As remarked in Section "An approximate solution", if the oxide layer is sufficiently thin $[h_{ox} \ll h_m]$, a good approximation can be obtained by assuming $\dot{\varepsilon}_m = 0$, which considerably simplifies the calculation. This approximation [dashed lines] is compared with the more precise calculation [solid lines] in Fig. 5 for the same conditions as in [6] and Fig. 4. The results show that the approximation of Section "An approximate solution" predicts stresses that are very close to those of the more exact calculation at $T = 923$ K, but that the approximation significantly overestimates the stress at $T = 983$ K.
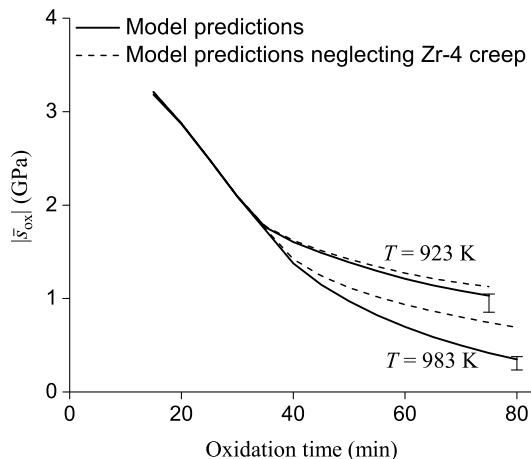


Figure 5: Comparison of predictions of the present model including substrate strains [solid line] and neglecting them [dashed line] at temperatures $T = 923$ K and $T = 983$ K. The dashed line is obtained from the approximation of Section "An approximate solution". Error bars represent the uncertainty in Zr-4 creep parameters.

The theoretical model of Platt *et al.* [6] attributes stress relaxation entirely to creep in the metal substrate. However, this leads to plausible predictions of oxide stresses only if (i) the initial stress in

12

the oxide is assumed to be $\sim 2$ GPa, which is lower than the measured stress magnitudes of Ref. [21, 22] and (ii) the creep rate is assumed to be much more rapid than reported data [23, 24]. Platt *et al.* [6] estimated substrate creep parameters using oxide strain measurements from experiments at $T = 633$ K [3], but our simulations recognizing the role of plastic deformation in the oxide show that creep in the substrate has a negligible effect at this temperature for the entire range of possible power-law creep strain rates of Zr-4. This is consistent with oxidation strain measurements of Ref [23, 24] at $T = 633$ K, which are in a range where only elastic behaviour is to be anticipated in the substrate.

## Stress distributions

Preuss *et al.* [9] measured the stresses *ex situ* at various depths within a 78 $\mu$m thick oxide layer that was formed on a ZIRLO sheet oxidized at 688 K for 600 days. Even though the stresses were measured only in the monoclinic phase ($s_M$), reported tetragonal content was less than 5% in the oxide layer, so these results can reasonably be compared with the current numerical model. In the absence of oxide growth data for intermediate points, a linear law (giving $h_{ox} = 78$ $\mu$m at $t = 600$ days) was assumed.
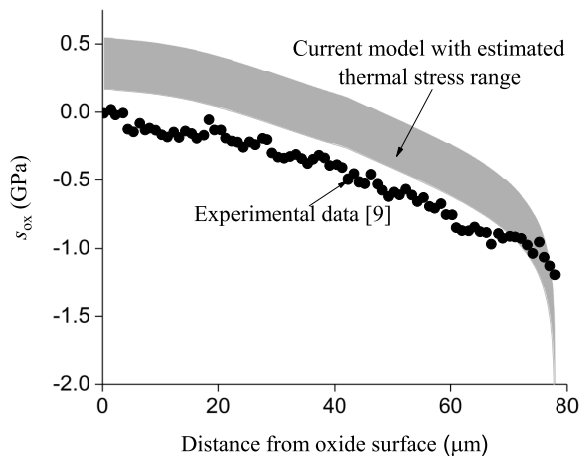


Figure 6: Comparison of predictions of in-plane oxide stress ($s_{ox}$) distribution across its thickness at $T = 688$ K with *ex-situ* experimental data for ZIRLO from [9]. The shaded region represents predicted results for the range $\alpha_{ox} = 5 \pm 2 \times 10^{-6}$ K$^{-1}$.

Figure 6 compares the predicted stress distribution with the experimental data from [9]. The shaded region defines the bounds of the predictions for $\alpha_{ox}$ in the range $5 \pm 2 \times 10^{-6}$ K$^{-1}$ (see Section "Thermal strain"); $\dot{\epsilon}_0 = 300$ s$^{-1}$ and nominal values of the creep rates of Zr-4 were assumed, in the

absence of suitable data for ZIRLO. The predicted range of the *ex situ* oxide stress and the form of the distribution agree well with the experimental results.

**Evolution of the stress distribution over time**

In view of the good agreement in Fig. 6, we performed additional simulations to track how the oxide stress distribution is predicted to evolve over time. Fig. 7a shows the evolution of the in-plane compressive stress distribution in the oxide as oxidation proceeds at 633 K, for which we used oxide growth data from [3]. The vertical straight lines represent the location of the metal-oxide interface at that particular instant of time. In each case the oxide is formed at very high compressive stress, but this relaxes rapidly to a value in the range $2 \sim 3$ GPa. Subsequent stress relaxation at any given point is then comparatively slow.
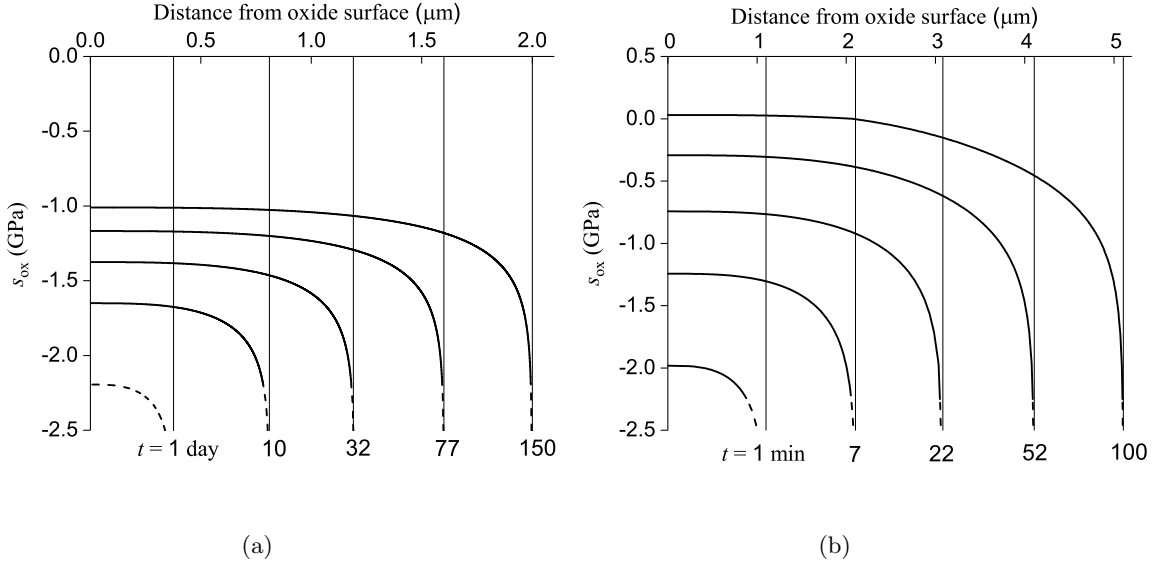


(a)                                                      (b)

Figure 7: Predicted in-plane stress distribution in the oxide layer at various times $t$ for (a) $T = 633$ K , and (b) $T = 973$ K. Vertical lines represent location of the metal-oxide interface at time $t$.

Figure 7(b) shows corresponding stress distributions at a temperature of 973 K, using oxide growth data from [25]. The higher temperature leads to faster rates of stress relaxation, resulting in larger stress gradients across the film. Note that XRD estimates of the average stress across the film may be weighted towards shallower depths in the oxide due to the partial absorption of rays coming from relatively deeper locations. With stress distributions of the form of Fig. 7, this would lead to an underestimate of the average stress. XRD penetration depends on tilt angle, incident angle and the

respective phase of the oxide [26], but in the absence of such detailed data, the theoretical results discussed in this paper were all plotted using an unweighted [uniform] average.

Figure 7 also shows that the stresses remain predominantly compressive up to the oxide-water interface for oxidation of 150 days at $T = 633$ K and 100 minutes at $T = 973$ K. These are approximately the times at which a transition in the oxidation kinetics is reported to occur at these temperatures [2, 3, 25]. Hence, there seems to be no possibility of formation of through-thickness vertical cracks that could provide a barrier-free path for oxidizing species to diffuse to the metal-oxide interface. This result is consistent with the SEM observations by Nakamura *et al.* [27], which show that no vertical cracks exist in the oxide film either before or immediately after the observed transition in the oxidation kinetics at $T = 773$ K.

## Other geometries

The discussion so far has mainly centered around the symmetric plate geometry of Fig. 1, but the constitutive behaviour for metal and oxide outlined in the section "Material behavior" could in principle be applied to any geometry, using a finite element implementation. Also, the solution of Section "An approximate solution" can be used in any situation where the oxide film thickness is sufficiently small compared with any other linear dimensions of the body.

The cladding tube used in PWRs is 570 $\mu$m thick and has a mean radius of 4.4 mm. It can therefore reasonably be treated as a thin-walled tube, implying (i) that hoop stresses will be approximately uniform through the substrate thickness, and (ii) that the mean hoop stress across substrate and oxide will be much larger than the pressures applied on the curved surfaces. Thus, conditions approximate quite closely to those in Fig. 1 and based on Fig. 5, Eqn. (12) provides a very convenient and quick estimate for the stress field provided the temperature is not too high.

## Conclusions

In this study, we have developed a stress evolution model for the oxide layers formed on zirconium alloys. Dislocation glide in the oxide layer and power-law creep in the substrate are proposed as the

most significant deformation mechanisms for the temperature range of $T = 600 - 1000$ K. Our thesis is that the oxide deforms primarily by dislocation glide for $T < 900$ K, while creep of the substrate only becomes significant at higher temperatures. This result is also consistent with the oxidation strain data reported in the literature [23, 24], which indicates that the substrate behaves elastically at $T = 633$ K.

All the model parameters were taken from the literature except the glide parameters $(Q_g, \sigma_g)$, which were assumed to be the same as for yttria-stabilized cubic zirconia. Direct experimental investigations of creep parameters for monoclinic and tetragonal zirconia are needed to validate applicability of these parameters to the oxide film as well, as to predict the stresses for $T > 1000$ K. The pre-exponential glide constant, $\dot{\epsilon}_0$, was estimated using a curve fit to experimental data for *ex-situ* oxide stresses, but uncertainty in the thermal strains within the oxide results leads to significant variability in this parameter. Further experimental investigation of the thermal stresses generated during temperature-cycling of oxide layers could enable more precise predictions to be made.

If the oxide film thickness is small compared with that of the substrate, a simple approximation to the stress field can be quickly obtained by assuming the in-plane strain rate to be zero.

# References

[1] M. Mamivand, M. A. Zaeem, H. El Kadiri, and L.-Q. Chen, "Phase field modeling of the tetragonal-to-monoclinic phase transformation in zirconia," *Acta Mater.*, vol. 61, no. 14, pp. 5223–5235, 2013. doi: https://doi.org/10.1016/j.actamat.2013.05.015.

[2] A. T. Motta, A. Couet, and R. J. Comstock, "Corrosion of zirconium alloys used for nuclear fuel cladding," *Annu. Rev. Mater. Res.*, vol. 45, pp. 311–343, 2015. doi: https://doi.org/10.1146/annurev-matsci-070214-020951.

[3] E. Polatidis *et al.*, "Residual stresses and tetragonal phase fraction characterisation of corrosion tested zircaloy-4 using energy dispersive synchrotron X-ray diffraction," *J. Nucl. Mater.*, vol. 432, no. 1-3, pp. 102–112, 2013. doi: https://doi.org/10.1016/j.jnucmat.2012.07.025.

[4] N. Petigny, P. Barberis, C. Lemaignan, C. Valot, and M. Lallemant, "In situ XRD analysis of the oxide layers formed by oxidation at 743 K on Zircaloy-4 and Zr-1NbO," *J. Nucl. Mater.*, vol. 280, no. 3, pp. 318–330, 2000. doi: https://doi.org/10.1016/S0022-3115(00)00051-9.

[5] F. Yang, X. Zhao, and P. Xiao, "In situ measurement of stresses and phase compositions of the Zirconia scale during oxidation of Zirconium by Raman spectroscopy," *Oxid. Met.*, vol. 81, no. 3-4, pp. 331–343, 2014. doi: https://doi.org/10.1007/s11085-013-9433-8.

[6] P. Platt *et al.*, "A study into stress relaxation in oxides formed on zirconium alloys," *J. Nucl. Mater.*, vol. 456, pp. 415–425, 2015. doi: https://doi.org/10.1016/j.jnucmat.2014.09.072.

[7] W. Qin, C. Nam, H. L. Li, and J. A. Szpunar, "Tetragonal phase stability in $ZrO_2$ film formed on zirconium alloys and its effects on corrosion resistance," *Acta Mater.*, vol. 55, no. 5, pp. 1695–1701, 2007. doi: https://doi.org/10.1016/j.actamat.2006.10.030.

[8] J. Chevalier, L. Gremillard, A. V. Virkar, and D. R. Clarke, "The tetragonal-monoclinic transformation in zirconia: lessons learned and future trends," *J. Am. Ceram. Soc.*, vol. 92, no. 9, pp. 1901–1920, 2009. doi: https://doi.org/10.1111/j.1551-2916.2009.03278.x.

[9] M. Preuss *et al.*, "Studies regarding corrosion mechanisms in zirconium alloys," *J. ASTM Int.*, vol. 8, no. 9, pp. 1–23, 2011. doi: https://doi.org/10.1520/JAI103246.

[10] P. Tejland and H.-O. Andrén, "Origin and effect of lateral cracks in oxide scales formed on zirconium alloys," *J. Nucl. Mater.*, vol. 430, no. 1-3, pp. 64–71, 2012. doi: https://doi.org/10.1016/j.jnucmat.2012.06.039.

[11] A. Ly *et al.*, "Understanding crack formation at the metal/oxide interface during corrosion of zircaloy-4 using a simple mechanical model," *J. ASTM Int.*, vol. 8, no. 9, pp. 1–18, 2011. doi: https://doi.org/10.1520/JAI103550.

[12] P. Platt, P. Frankel, M. Gass, and M. Preuss, "Critical assessment of finite element analysis applied to metal–oxide interface roughness in oxidising zirconium alloys," *J. Nucl. Mater.*, vol. 464, pp. 313–319, 2015. doi: https://doi.org/10.1016/j.jnucmat.2015.05.002.

[13] H. Wang, Z. Hu, W. Lu, and M. D. Thouless, "A mechanism-based framework for the numerical analysis of creep in Zircaloy-4," *J. Nucl. Mater.*, vol. 433, no. 1, pp. 188–198, 2013. doi: https://doi.org/10.1016/j.jnucmat.2012.08.049.

[14] M. Guerain, C. Duriez, J. L. Grosseau-Poussard, and M. Mermoux, "Review of stress fields in Zirconium alloys corrosion scales," *Corros. Sci.*, vol. 95, pp. 11–21, 2015. doi: https://doi.org/10.1016/j.corsci.2015.03.004.

[15] H. J. Frost and M. F. Ashby, *Deformation-mechanism maps: The plasticity and creep of metals and ceramics.* Oxford, UK: Pergamon Press, 1982. ISBN 9780080293370

[16] D. Kaddour *et al.*, "Experimental determination of creep properties of zirconium alloys together with phase transformation," *Scr. Mater.*, vol. 51, no. 6, pp. 515–519, 2004. doi: https://doi.org/10.1016/j.scriptamat.2004.05.046.

[17] A. H. Chokshi, "Diffusion, diffusion creep and grain growth characteristics of nanocrystalline and fine-grained monoclinic, tetragonal and cubic zirconia," *Scr. Mater.*, vol. 48, no. 6, pp. 791–796, 2003. doi: https://doi.org/10.1016/S1359-6462(02)00519-5.

[18] D. L. Douglass, "Oxide plasticity in the oxidation mechanism of zirconium and its alloys," *Corros. Sci.*, vol. 5, no. 4, pp. 255–268, 1965. doi: https://doi.org/10.1016/S0010-938X(65)90592-5.

[19] B. Baufeld, B. V. Petukhov, M. Bartsch, and U. Messerschmidt, "Transition of mechanisms controlling the dislocation motion in cubic $ZrO_2$ below 700 °C," *Acta Mater.*, vol. 46, no. 9, pp. 3077–3085, 1998. doi: https://doi.org/10.1016/S1359-6454(98)00007-X.

[20] M. Parise, O. Sicardy, and G. Cailletaud, "Modelling of the mechanical behavior of the metal-oxide system during Zr alloy oxidation," *J. Nucl. Mater.*, vol. 256, no. 1, pp. 35–46, 1998. doi: https://doi.org/10.1016/S0022-3115(98)00045-2.

[21] T. Arima, T. Masuzumi, H. Furuya, K. Idemitsu, and Y. Inagaki, "The oxidation kinetics and the structure of the oxide film on Zircaloy before and after the kinetic transition," *J. Nucl. Mater.*, vol. 294, no. 1-2, pp. 148–153, 2001. doi: https://doi.org/10.1016/S0022-3115(01)00453-6.

[22] Y.-S. Kim, Y.-H. Jeong, and J.-N. Jang, "Stress measurements during thin film zirconium oxide growth," *J. Nucl. Mater.*, vol. 412, no. 2, pp. 217 – 220, 2011. doi: https://doi.org/10.1016/j.jnucmat.2011.03.001.

[23] M. Blat-Yrieix *et al.*, "Toward a better understanding of dimensional changes in Zircaloy-4: what is the impact induced by hydrides and oxide layer?" in *Zirconium in the Nucl. Industry: 15th Int. Symp.* ASTM Int., 2009, pp. 594–611.

[24] A. T. Donaldson, "Growth in Zircaloy-4 fuel clad arising from oxidation at temperatures in the range 623 to 723 K," in *Zirconium in the Nucl. Industry: Ninth Int. Symp.* ASTM Int., 1991, pp. 177–197.

[25] S. Leistikow, G. Schanz, H. V. Berg, and A. E. Aly, "Comprehensive presentation of extended Zircaloy-4 steam oxidation results (600-1600 deg. C)," Dep. Metallurgy, Atomic Energy Commission of Egypt, Cairo, Egypt, Tech. Rep. IWGFPT–16, 1983.

[26] I. C. Noyan and J. B. Cohen, *Residual stress: measurement by diffraction and interpretation.* New York, USA: Springer-Verlag, 1987. ISBN 9780387963785

[27] J. Nakamura, M. Hashimoto, T. Otomo, and S. Kawasaki, "Effects of oxygen partial pressure on oxidation of Zircaloy," *J. Nucl. Mater.*, vol. 200, no. 2, pp. 256–264, 1993. doi: https://doi.org/10.1016/0022-3115(93)90336-W.